J. Plasma Fusion Res. SERIES, Vol. 3 (2000) 3–9

Progress in LHD Experiment

MOTOJIMA Osamu*, OHYABU Nobuyoshi, KOMORI Akio, KANEKO Osamu, YAMADA Hiroshi, KAWAHATA Kazuo, ASHIKAWA Naoko[1], CHIKARAISHI Hirotaka, DEVRIES Peter, EMOTO Masahiko, FUNABA Hisamichi, GOTO Motoshi, HAMAGUCHI Shinji, IDA Katsumi, IDEI Hiroshi, IMAGAWA Shinsaku, INAGAKI Shigeru, INOUE Noriyuki, IWAMOTO Akifumi, KADO Shinichiro, KITAGAWA Shiro, KUBO Shin, KUBOTA Yusuke, KUMAZAWA Ryuhei, MAEKAWA Ryuji, MASUZAKI Suguru, MINAMI Takashi, MITO Toshiyuki, MIYAZAWA Junichi, MORISAKI Tomohiro, MORITA Shigeru, MURAKAMI Sadayoshi, MUTO Sadatsugu, MUTOH Takashi, NAGAYAMA Yoshio, NAKAMURA Yukio, NAKANISHI Hideya, NARIHARA Kazumichi, NISHIMURA Arata, NISHIMURA Kiyohiko, NODA Nobuaki, KOBUCHI Takashi[1], OHDACHI Satoshi, OKA Yoshihide, OSAKABE Takeshi, OZAKI Tetsuo, PETERSON Byron, SAGARA Akio, SAITOH Kenji[2], SAKAKIBARA Satoru, SAKAMOTO Ryuichi, SASAO Hajime[1], SASAO Mamiko, SATO Kuninori, SATO Motoyasu, SEKI Tetsuo, SHIMOZUMA Takashi, SHOJI Mamoru, SUZUKI Hajime, TAKAHATA Kazuya, TAKECHI Manabu[2], TAKEIRI Yasuhiko, TAMURA Hitoshi, TAMURA Naoki, TANAKA Kenji, TOI Kazuo, TOKUZAWA Tokihiko, TSUMORI Katsuyoshi, TSUZUKI Kazuhiro, YAMADA Ichihiro, YAMADA Syuichi, YAMAGUCHI Satarou, YAMAMOTO Satoshi[2], YANAGI Nagato, YOKOYAMA Masayuki, WATANABE Kiyomasa, WATARI Tetsuo, HAMADA Yasuji, ITOH Kimitaka, MATSUOKA Keisuke, MURAI Katsuji, OHKUBO Kunizo, SATOH Sadao, SATOW Takashi, SUDO Sigeru, TANAHASHI Shyugo, YAMAZAKI Kozo, OHTAKE Isao, AKIYAMA Ryuuichi, HABA Kiichiro, IIMA Masashi, KODAIRA Jun-ichi, TSUZUKI Tetsuya and FUJIWARA Masami

National Institute for Fusion Science, Toki, Gifu-ken, 509-5292, Japan

[1]*Graduate University for Advanced Studies, Hayama, 240-0193, Japan*

[2]*Department of Energy Engineering and Science, Nagoya University 464-8603, Japan*

(Received: 25 February 2000 / Accepted: 19 June 2000)

Abstract

In the third campaign (07.13.99–12.14.99), NBI (≤4.2 MW), ICRH (≤1.4 MW) and ECRH (≤0.9 MW) were used to heat the plasma in LHD. The carbon tiles were installed as divertor plates, resulting in significant reduction in metal impurity concentration (Fe). The maximum field used in the experiment is 2. 9 T. Upgrading of the key hardware systems led to (i) higher T_e [$T_e(0)$ = 4.4 keV at $\bar{n}_e = 5.3 \times 10^{18}$ m^{-3} and P_{abs} = 1.8 MW], (ii) higher confinement [τ_E = 0.3 s, $T_e(0)$ = 1.1 keV at $n_e(0) = 6.5 \times 10^{19}$ m^{-3} and P_{abs} = 2.0 MW], (iii) higher stored energy W_p = 880 kJ, (iv) higher volume averaged $\bar{\beta}$ = 2.4% (at B = 1.3 T). The temperature pedestal enhances the confinement significantly (50% higher than the ISS95 scaling). The ICRH heating was found to be as efficient as NBI heating. Long pulse discharges (80 sec NBI shot, 68 sec ICRH shot) have been achieved without any technical difficulty.

Keywords:

toroidal confinement device, helical device, plasma heating, divertor, high temperature plasma, confinement time, pedestal

*Corresponding author's e-mail: motojima@LHD.nifs.ac.jp

1. Introduction

The Large Helical Device (LHD) is a large heliotron type superconducting device with divertor [l = 2, m = 10, R_{ax} (position of magnetic axis) = 3.6–3.9 m, a (minor radius) = 0.6 m, B = 3 T]. The LHD experiment began in March 1998 after its eight-year construction [1-3]. The major goals of the LHD experiments are: (i) Physics experiment from which break even condition can be extrapolated ($nT\tau_E > 10^{20}$ keVm^{-3}s (Q~0.35), $T >$ 10 keV, $\bar{\beta} > 5\%$), (ii) demonstration of advanced toroidal plasma operation, i.e., disruption free steady state operation of current less helical plasma with divertor.

In Table 1 we summarize the plasma parameters achieved during the 3rd campaign of the LHD experiment in 1999. Achieved data points of the plasma-stored energy are compared with tokamak H-mode database in Fig. 1. Considering the smaller heating power and plasma volume, the present data of the LHD are very promising. In this paper, we describe the key physics areas with good progress.

2. ICRF Heating

Up to now, NBI has been the main power source to heat the LHD plasmas. But in the 3rd campaign, we executed successfully ICRF heating experiment (1.3 MW, 38.47 MHz). The gas used in the experiment is helium with hydrogen as a minority species. When ICRF power was applied to ECRH generated target plasma, the stored energy and the temperature increased while the density was kept nearly constant. The plasma parameters were: $\bar{n}_e$ (line averaged electron density) = 5 × 10^{18} m^{-3}, W_p (plasma stored energy) = 200 kJ, $T_e(0)$ = 1.6–2.0 keV, P_{ICRF} = 1.25 MW and such a plasma was maintained stably for 5 seconds by ICRF power alone without any impurity problem. Moreover, when ICRF power of 1.3 MW is added to the NBI (1.4 MW) heated plasma, the stored energy increased from 270 kJ to 420 kJ, accompanying electron temperature rise of 0.5 keV. Such heating experiments clearly demonstrated that the heating efficiency was similar to that of NBI heating.

Table 1 Plasma parameters achieved during the 3rd campaign (1999).

High Electron Temperature	$T_e(0)$	4.4 keV
	$T_i(0)$	2.7 keV
	τ_E	0.06 s
	P_{abs}	1.8 MW
	$\bar{n}_e$	5.3 × 10^{18} m^{-3}
High Ion Temperature	$T_e(0)$	3.3 keV
	$T_i(0)$	3.5 keV
	τ_E	0.09 s
	P_{abs}	3.9 MW
	$\bar{n}_e$	1.0 × 10^{19} m^{-3}
High Confinement	$T_e(0)$	1.1 keV
	τ_E	0.3 s
	P_{abs}	2.0 MW
	$n_e(0)$	6.5 × 10^{19} m^{-3}
	$n_e(0)\tau T_e(0)$ = 2.0 × 10^{19} keVm^{-3}s	
Maximum Stored Energy	880 kJ	
Highest Beta (volume averaged)	$\bar{\beta}$	2.4% at B_t = 1.3 T
Maximum Density	$\bar{n}_e$	1.1 × 10^{20} m^{-3}

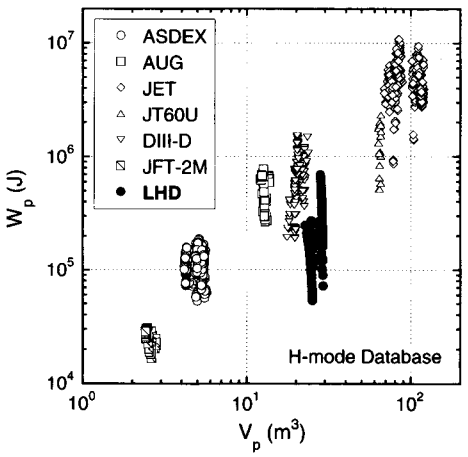

Fig. 1 Achieved plasma energy of LHD in comparison with Tokamak H-mode database.

3. Generation of High Temperature Plasmas

To achieve high central temperature, we used RF heating. Central ECH heating (168 GHz, second harmonics) requires B = 2.9 T for the inward shifted configuration (R_{ax} = 3.6 m). The temperature profiles at $\bar{n}_e$ = 5 × 10^{18} m^{-3} are shown in Fig. 2. The ion temperature, measured by Doppler shift of the impurity line was 2.7 keV. The electron resonance heating resulted in more peaked electron temperature profile compared with the profiles of the NBI heated discharges and the central value was as high as 4.4 keV. Figure 3 shows the central electron temperature achieved with presently available RF power as a function of the density. At very low density ($\bar{n}_e$ < 2 × 10^{18} m^{-3}), the temperature became even higher. With combination of NBI and ICRF heating, we achieved the central ion

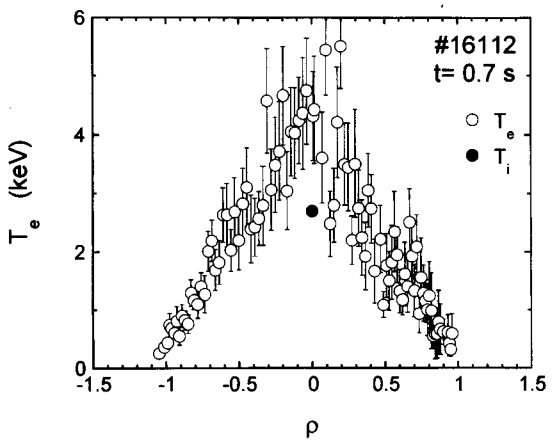

Fig. 2 Temperature profile of a discharge heated by ECH and ICRF.

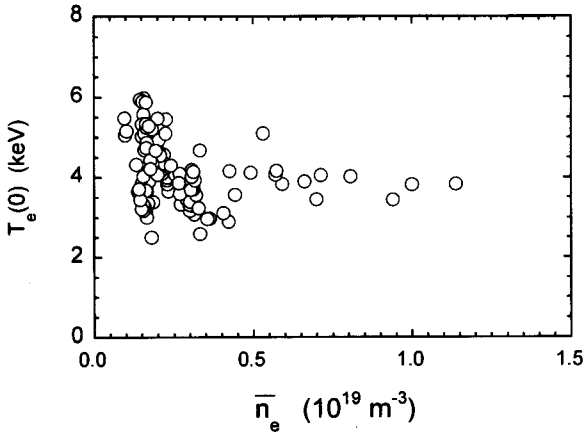

Fig. 3 Density dependence of the central electron temperature of the discharges heated by ECH and ICRF.

temperature of 3.5 keV and the profiles are shown in Fig. 4. The electron temperature was found to be nearly equal to that of the ions. The edge temperatures at ρ (normalized radius) = 0.85 were as high as 1.3 keV [4,5]. Such high edge temperatures are believed to result in improvement in confinement over the stellarator scaling (ISS95) [4,6].

4. Energy Confinement Scaling

Early experimental results have shown that the energy confinement time of the LHD is significantly better than the value predicted by the scaling based on data set from the small heliotron typed devices [2,3,6]. We have accumulated the confinement data and comparison with other devices is given in Fig. 5. The

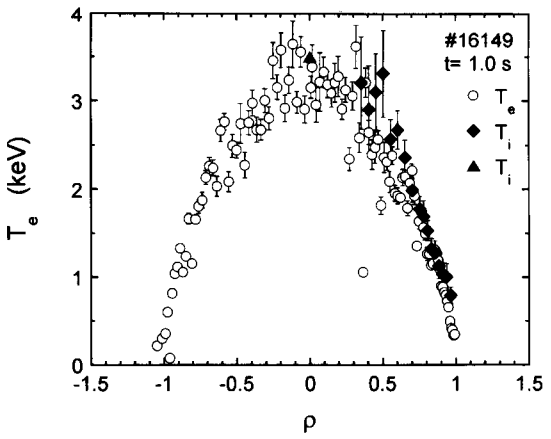

Fig. 4 Ion and electron temperature profiles of a discharge heated by NBI and ICRF.

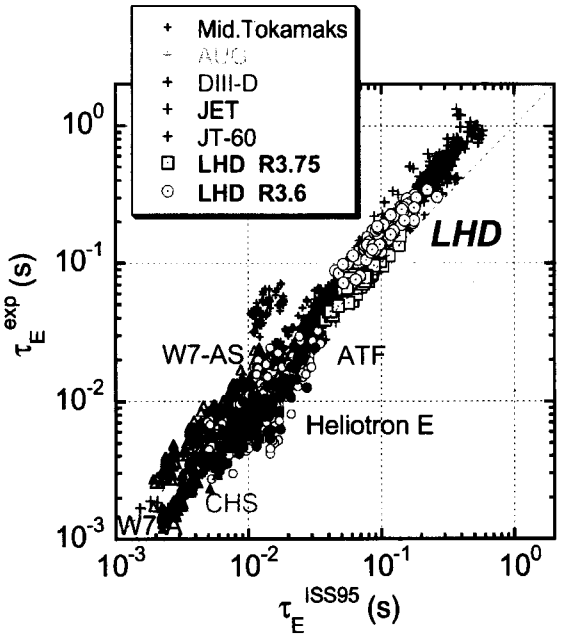

Fig. 5 Comparison between experimental values of energy confinement and those predicted from ISS95 scaling. (tokamak data from ITER H-mode Database, Ver.5)

discharge with the inward shifted configuration (R_{ax} = 3.6 m) exhibits a factor of 1.6 improvements over the ISS95 scaling and the confinement is comparable to those of ELMy H-mode tokamaks. The observed high edge temperature, not seen in the smaller heliotron devices resulted in higher stored energy and hence higher energy confinement. One of the main experimental goals is to maintain such a level of improvement factor or even to enhance improvement

factor in the near future experiment with high heating power.

5. Edge Transport Barrier

Edge transport barrier was observed in the LHD discharges [4,5]. The barrier or pedestal forms during the plasma pressure increasing phase, not through a rapid transition as in tokamak H-mode. With beam heating on, the hot plasma region expands radially and eventually reaches the last closed magnetic surface (LCMS) and divertor plates. During this process, T_e^{ped} (the electron temperature at the shoulder of the pedestal, (ρ = 0.85–0.9) increases naturally, forming an edge temperature pedestal. A clear pedestal can be seen in Fig. 4. The estimated total thermal conductivity ($n_e\chi$) there is fairly low, typically 1.0–2.0 × 10^{19} $m^{-1}s^{-1}$ and thus transport in this edge region can be called an edge thermal transport barrier. Unlike tokamak H-mode barriers, the particle (including the impurity ions) confinement does not appear to improve and furthermore there is no sign of the ELM.

For the low-density discharges, the temperature at the pedestal becomes as high as 1.3 keV. The width of the pedestal (Δ) averaged over the flux surface is found to be 6 cm, which is much wider than that of the comparable tokamak. One of the amazing features of the LHD edge barrier is that the pedestal temperature is found to be close to the averaged temperature ($<T_e>$) [the temperature ratio ($T_e^{ped}/<T_e>$) can be as high as 0.8]. Thus W_p is almost proportional to $n_eT_e^{ped}$ and thus the edge confinement almost determines τ_E (the global energy confinement time). The density dependences of $T_e(0)$ and T_e^{ped} (at the fixed input power) are depicted in Fig. 6(a). Both central and pedestal temperatures decrease gradually with increasing density, leading to higher stored energy at higher density. When $\bar{n}_e$ is below 3 × 10^{19} m^{-3}, T_e^{ped} exceeds 1 keV. Fig. 6(b) shows power dependences of $T_e(0)$ and Teped for a fixed density (n~4.4 × 10^{19} m^{-3}). Both temperatures increase rapidly with input power when P is below 2 MW. In higher power regime, however, the increment of T_e^{ped} with power is modest. This is the main issue, which we have to solve experimentally. Optimistically, further increased power in the near future experiment could naturally lead to the better confinement regime or mode. With modification of the divertor from open to closed configuration, we are planning a more drastic edge control (combination of the pellet or beam fueling and high efficient pumping) for confinement enhancement. A possible scenario of pedestal formation is that the

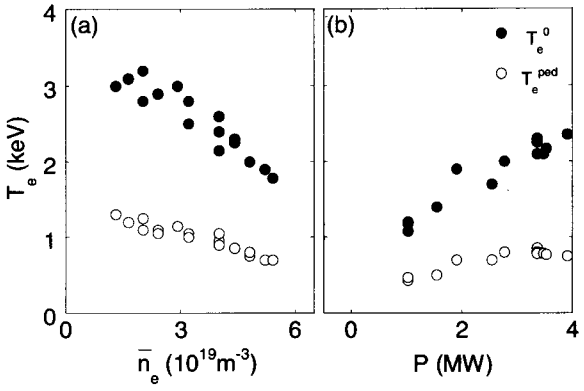

Fig. 6 Parametric dependences of T_e^0 and T_e^{ped} (a) Density dependence (P = 3.3 MW, B = 2.75 T), (b) Power dependency ($\bar{n}_e$ = 4.4 × 10^{19} m^{-3}, B = 2.75 T).

$\iota/2\pi$ = 1 surface or its associated island could play a major role in formation of the edge pedestal since the $\iota/2\pi$ = 1 surface was always located within or just outside the pedestal region for the configurations tested so far. It is also important to notice that the inherent features of the LHD magnetic geometry such as "reverse" shear, high shear at the edge and short connection length between good and bad curvature regions may be key factors for the barrier mechanism. Better understanding of the barrier certainly requires more detailed experimental study together with theoretical works.

6. Radial Electric Field

The radial electric field is the key parameter for confinement of the collisionless helical plasmas [7]. The transition from ion root (negative radial electric field) to electron root (positive radial electric field) was observed in plasmas with NBI heating at the low density of 0.4 – 1.0 × 10^{19} m^{-3} in LHD. The radial electric field is derived from the poloidal and toroidal rotation velocity and pressure gradient of Neon impurity measured with charge exchange recombination spectroscopy using radial force balance. Since the toroidal rotation was damped to less than 10 km/s due to the toroidal viscosity and the effect of diamagnetic drift velocity was also small due to the high Z of Neon, the radial electric field was mainly determined by the poloidal rotation velocity. The radial electric field was negative (ion root) at the electron density larger than 1.0 × 10^{19} m^{-3}, while it became positive especially near the plasma edge at the low density below 1.0 × 10^{19} m^{-3}. Figure 7(a) shows the density dependence of radial electric field near the

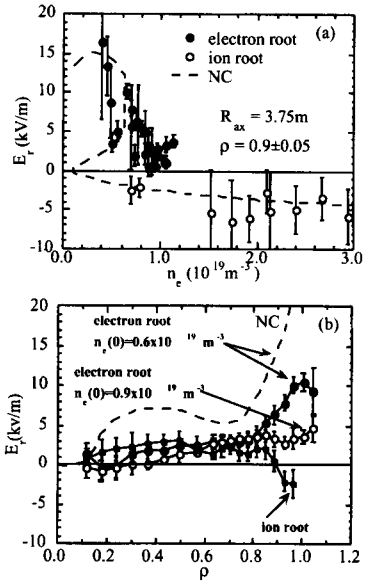

Fig. 7 Density dependence of radial electric field near the plasma edge (ρ = 0.9) and (b) radial profiles of radial electric in the density region at the transition from ion root to electron root for the plasmas.

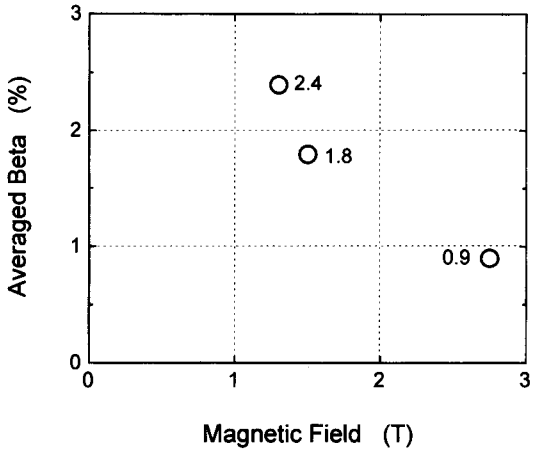

Fig. 8 Maximum achieved $\bar{\beta}$ value as a function of magnetic field.

plasma edge (ρ = 0.9) for the plasma heated by NBI with the magnetic axis of 3.75 m. In these plasmas, the central ion temperature was close to the central electron temperature (70–100% of central electron temperature). The edge radial electric field increased up to 15 kV/m in the electron root as the electron density was decreased to 0.4×10^{19} m^{-3}, while it was almost constant and to be –5 kV/m in the ion root in the wide range of electron density of $1.0 - 3.0 \times 10^{19}$ m^{-3}. The transition from ion root to electron root was observed at $\rho > 0.8$ and there was no large radial electric field observed in the plasma core (see Fig.7(b)). Since anomalous heat transport dominated over the neoclassical transport in our discharges, the transition was not accompanied by any observable change in confinement.

7. Achievement of High β Plasma and MHD Stability

In the 2nd campaign, the target plasmas were generated by second harmonics of ECH (84 GHz, 82.6 GHz) and then heated by NBI power. The magnetic field is strictly restricted to be 1.5 T. But we found that with well-conditioned wall NBI alone can initiate plasma with appropriate gas puffing and heat the plasma even without ECH [8,9]. This is a new plasma initiation scheme and allowed us to operate the discharges at any magnetic field (above B = 0.5 T). In the 3rd campaign, high $\bar{\beta}$ plasmas were achieved in the low field discharges, as depicted in Fig. 8 where the achieved $\bar{\beta}$ values at the various fields are plotted. At B = 1.3 T, $\bar{\beta}$ value estimated by diamagnetic signal reached 2.4% with help of pellet injection. With gas puffing, slightly lower value of beta, 2.1% was maintained for 1 second. The achieved value was limited by heating power, not by any kind of MHD instability. The inward shifted configuration exhibited higher confinement. In the LHD design phase, it has been believed that such a configuration is unstable to the ideal interchange mode even though it has better particle orbit properties and larger plasma volume compared with the standard configuration (R_{ax} = 3.75 m). We did not observe that any MHD activity influenced the plasma transport even the maximum $\bar{\beta}$ value of 2.4% was achieved. However, small magnetic fluctuations with various modes appeared as the $\bar{\beta}$ value increased (Fig. 9). Even though the amplitudes were small, but their appearance seems to be consistent with linear analysis of the interchange modes. Non-linear analyses of these modes are definitely needed for understanding of the modes.

8. Deposition Profile of the Divertor Heat and Particle Flows

The LHD discharges are equipped with open helical divertor configuration. In the 1st and 2nd campaigns in 1998, all plasma facing materials were stainless steel including divertor plates In the 3rd campaign, the carbon tiles were used as divertor plates, resulting in significant reduction in metal impurity (Fe)

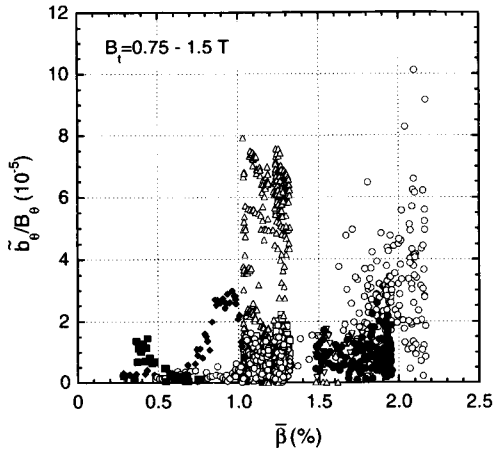

Fig. 9 Change in mode amplitude as a function of $\bar{\beta}$. Various MHD mode has been observed and the amplitude approaches about 10^{-4}. Strong instabilities which affect plasma confinement have not been observed so far.

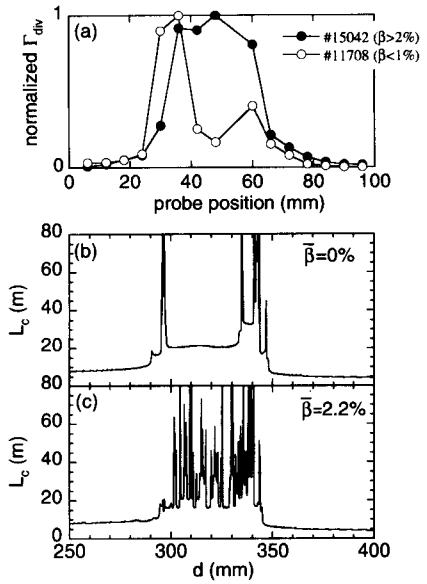

Fig. 10 Heat deposition profiles on the divertor plate for low $\bar{\beta}$ and high $\bar{\beta}$ (2.2%) discharges. (b), (c) The connection length on the divertor plate for zero and 2.2% $\bar{\beta}$ configurations. (Calculated by field line tracing code).

and its associated radiative power. Mainly electrostatic probes diagnose the divertor plasma. Since the LHD divertor magnetic configuration has a 3-dimensional structure, the divertor/SOL structure is not a simple layer as in tokamak. In some cases, the split layers with a few cm gaps strike the divertor plates. An example is shown in Fig. 10. The connection length, defined as a field line length from a position on the divertor plate to the other divertor plates is calculated by field line trace code (Fig. 10(b, c)). It predicts that two split layer structure for low $\bar{\beta}$ configuration becomes one with many layers for high $\bar{\beta}$ configuration. This is confirmed by the probe measurements (Fig. 10(a)). The divertor temperature and density measured by probes on the divertor plates were typically 5–40 eV and $0.1 - 5.0 \times 10^{18}$ m^{-3}, respectively. The maximum operational densities were 1.2×10^{20} m^{-3} for the pellet fuelled discharge and 9×10^{19} m^{-3} with He gas puff alone. Even at the high-density regime, the divertor density is almost proportional to the line averaged density and hence high recycling divertor plasma observed in the tokamak (strong non-linear dependence of the divertor density on the line averaged density) was not observed. It is interesting to see whether such divertor plasma behavior persist even in the high power experiment.

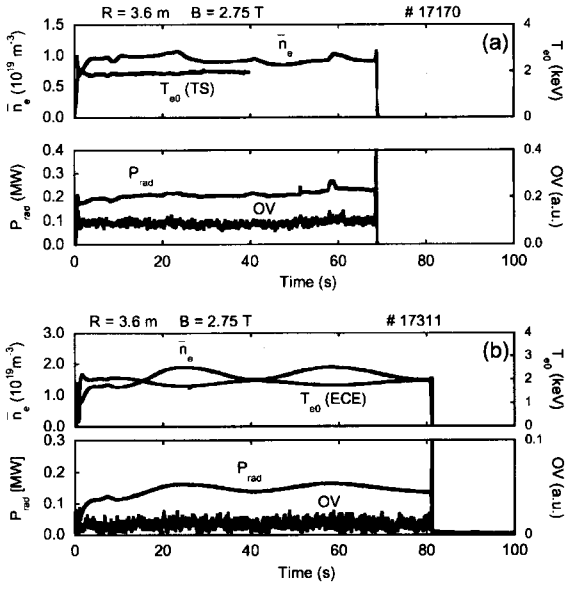

Fig. 11 (a) Long pulsed discharge heated and maintained by ICRF heating alone, (b) Long pulsed discharge heated and maintained by NBI heating alone.

9. Long Pulse Discharges

Demonstration of steady-state helical plasma with high quality is one of the major goals in the LHD experiment. In the 3rd campaign, we installed carbon tile divertor plates, which made long pulse discharge possible. Figure 11 shows the time evolutions of two discharges, heated by ICRF (1 MW) and NBI (0.5 MW)

respectively. They lasted more than 1 minute. In both discharges, the electron densities were $1–2 \times 10^{19}$ m^{-3} and were controlled by manual gas puffing. The electron temperature was kept to be around 1–2 keV. The radiation power is less than 20% of the input power and no sign of the impurity accumulation. These discharges were terminated by minor hardware problems of the heating systems. In near future, we plan to operate even longer discharges with higher input power.

10. Summary

LHD experiment is progressing well with improved plasma parameters in Table 1 and Fig. 1 and many fruitful physics results. The rapid progress of the plasma parameters is realized by the disruption free property of the LHD magnetic configuration and technical advantages of superconducting device. The LHD experiment is now exploring a new regime for toroidal magnetic confinement with current less plasma, which is the least free energy configuration. It will provide valuable database with the wide dynamic range to the plasma physics and controlled fusion research.

References

[1] A. Iiyoshi, A. Komori, A. Ejiri *et al.*, Nucl. Fusion **39**, 1245 (1999).

[2] M. Fujiwara, H. Yamada, M. Emoto *et al.*, Nucl. Fusion **39**, 1659 (1999).

[3] O. Motojima, H. Yamada. A. Komori *et al.*, Phys. Plasma **6**, 1843 (1999).

[4] N. Ohyabu, K. Narihara, H. Funaba *et al.*, Phys. Rev. Lett. **84**, 103 (2000).

[5] N. Ohyabu, A. Fujisawa, N. Ashikawa *et al.*, to appear in Phys. Plasma, (2000).

[6] H. Yamada, K.Y. Watanabe, S. Sakakibara *et al.*, Phys. Rev. Lett. **84**, 1216 (2000).

[7] O. Motojima, T. Mutoh, M. Sato *et al.*, Nuclear Fusion Supplement 1 (1989) 551 (IAEA-CN-50/E-I-4).

[8] M. Fujiwara, O. Kaneko, A. Komori, *et al.*, to appear in Plasma Physics and Controlled Fusion 41 Supplement 12B, B157 (1999).

[9] O. Kaneko, Y. Takeiri, K. Tsumori *et al.*, Nucl. Fusion **39**, 1087 (1999).